Applied Surface Science 396 (2017) 1231–1238

Applied Surface Science

journal homepage: www.elsevier.com/locate/apsusc

Full Length Article

Time-resolved imaging of flyer dynamics for femtosecond laser-induced backward transfer of solid polymer thin films

M. Feinaeugle[a,*], P. Gregorčič[b], D.J. Heath[a], B. Mills[a], R.W. Eason[a]

[a] Optoelectronics Research Centre, University of Southampton, Southampton, SO17 1BJ, UK
[b] Faculty of Mechanical Engineering, University of Ljubljana, Aškerčeva 6, 1000, Ljubljana, Slovenia

ARTICLE INFO

Article history:
Received 15 July 2016
Received in revised form 27 October 2016
Accepted 15 November 2016
Available online 19 November 2016

Keywords:
Laser-induced backward transfer
Time-resolved shadowgraphy
Femtosecond laser-induced
micro-processing
Polymer thin films
Additive manufacturing
SU-8

ABSTRACT

We have studied the transfer regimes and dynamics of polymer flyers from laser-induced backward transfer (LIBT) via time-resolved shadowgraphy. Imaging of the flyer ejection phase of LIBT of 3.8 μm and 6.4 μm thick SU-8 polymer films on germanium and silicon carrier substrates was performed over a time delay range of 1.4–16.4 μs after arrival of the laser pulse. The experiments were carried out with 150 fs, 800 nm pulses spatially shaped using a digital micromirror device, and laser fluences of up to 3.5 J/cm^2 while images were recorded via a CCD camera and a spark discharge lamp. Velocities of flyers found in the range of 6–20 m/s, and the intact and fragmented ejection regimes, were a function of donor thickness, carrier and laser fluence. The crater profile of the donor after transfer and the resulting flyer profile indicated different flyer ejection modes for Si carriers and high fluences. The results contribute to better understanding of the LIBT process, and help to determine experimental parameters for successful LIBT of intact deposits.

1. Introduction

Additive methods for the microfabrication of devices have recently gained interest over conventional techniques due to their versatility, simplicity and resulting high speed of fabrication [1–3]. Among these, laser-based techniques are a promising way to enable device printing in a contactless fashion with demonstrated micron-scale resolution. A unique advantage is that these methods allow the deposition of materials that not only have a specific structural role, but also have electronic, photonic or even biomedical functionality.

In particular, laser-induced forward transfer (LIFT) has proven its capability to allow manufacturing of a wide range of materials, such as metals [4], ceramics, semiconductors, superconductors [5], 2D materials and structures for e.g. MEMS [6], waveguides [7], biomedical sensors [8] or thermoelectric generators [9]. More recently, the transfer of silver pastes [10,11], 3-dimensional micro-objects [12,13] and metal vias [14] has shown the potential of LIFT for microfabrication. During LIFT (e.g. with a transparent donor), shown schematically in Fig. 1a, a pulsed laser beam is focussed or imaged at the interface between a transparent carrier substrate and a sandwich of thin films, consisting of an absorbing material and the donor. As a consequence of the absorbed laser energy, a small volume of the donor is ejected and transferred onto a receiver substrate which is located parallel to the donor surface. In some cases, the donor itself acts as an absorber and no additional interfacial layer is required. The spacing between the donor and receiver is typically in the few to tens of micrometres range.

The minimum feature sizes of structures fabricated via LIFT is mainly limited to optical resolutions for congruent transfer of devices [15,16]. However, for molten transfer, structures that are smaller than the diffraction-limited size of the incident laser pulse have been demonstrated [17,18]. Specifically for the fabrication of those structures, laser-induced backward transfer (LIBT) [19] has produced submicron-structures with high repeatability which may prove to be an advantageous alternative to LIFT for specific applications [20,21]. During LIBT, shown schematically in Fig. 1b, the receiver whose absorption is low in comparison with the carrier is situated in the path of the laser, while the donor is coated on a (bulk) carrier substrate. The incident laser pulse energy that is either absorbed in the donor or- for partially transparent donors- the carrier leads to the transfer of a volume of the donor in a direction opposite to that of the laser beam path, hence the term 'backward'.

* Corresponding author. Current address: Chair of Applied Laser Technology, Laboratory of Mechanical Automation and Mechatronics, Faculty of Engineering Technology, University of Twente, Enschede, The Netherlands.
E-mail addresses: m.feinaeugle@utwente.nl (M. Feinaeugle), bm602@orc.soton.ac.uk (B. Mills).

http://dx.doi.org/10.1016/j.apsusc.2016.11.120

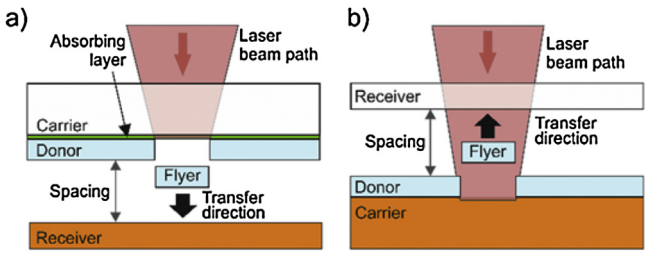

Fig. 1. Schematic side-view of (a) laser-induced forward transfer (LIFT) and (b) laser-induced backward transfer (LIBT) for a transparent donor.

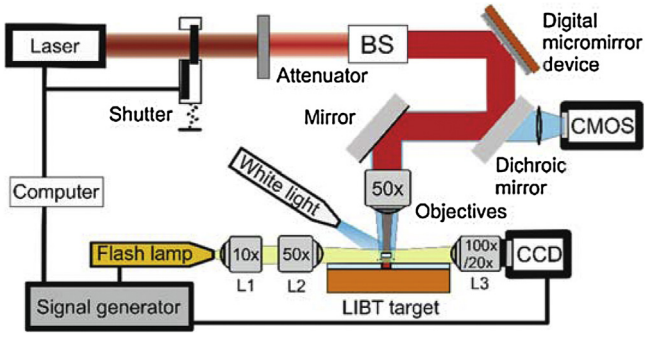

Fig. 2. Setup for time-resolved imaging of LIBT. The laser pulses with Gaussian beam profile are homogenised to a top hat profile via a refractive beam shaper (BS). Laser triggering, time-resolved imaging, DMD mask display and beam attenuation are controlled by a computer.

In comparison with LIFT, LIBT has different requirements and restrictions concerning the transparency of the receiver and the donor, but the possibility to use a bulk carrier substrate might prove advantageous for certain applications. These advantages can also be used for transfer of other materials as demonstrated in previous work, where metals [22–25], oxides [25,26], CrSi2 [27], TiN [24] and corroded surfaces [28] have been the subject of studies of LIBT methods.

Recently, we have demonstrated that the use of a bulk substrate facilitates the imprint-based laser-induced fabrication of sub-micron-size structures via LIBT of solid polymers [29].

While LIFT has been the object of many studies to date, much less effort has been put into fully understanding and exploiting the process of LIBT. To help in predicting the outcome of an experiment via LIBT e.g. with a new material, imaging [24] and simulation [30] of the process can be useful tools. Also, as LIBT is closely related to the processes of laser lift-off [31], laser cleaning, laser scribing, or even ablation [32], studying LIBT could also aid in understanding these processes. The main difference with respect to previous work is that for our experiments, we are interested in the ejected material being in an intact state, and that its shape is geometrically similar to the incoming spatial shape of the laser pulse.

To improve the effectiveness of LIBT, factors such as low flyer velocity and reduced shock generation play a major role in transferring a flyer in an intact state [33]. An experimental time-resolved imaging study could therefore support future efforts to model the LIBT process to optimise experimental conditions, and to understand the advantages and limitations of this technique. Previously, the femtosecond laser ablation of silica grown on top of silicon was investigated in the first ~10 ns after the arrival of the laser pulse [34]. In a different study, a simple model of silica on a Ag substrate was simulated on a picosecond timescale [30].

While the focus of those studies was on the observation of shock and film dynamics in the first nanoseconds after the arrival of the laser pulse, here, we have examined the dynamics of the emerging flyer and fragments on a microsecond scale to obtain experimental parameters for LIBT of intact deposits.

In this study, we have imaged the LIBT process from an epoxy-based SU-8 polymer donor film from planar silicon and germanium carriers via a femtosecond pulsed laser source. SU-8 is an example of a transparent donor material that can be used for e.g. photonic or microfluidic devices. This polymer, once developed, has a relatively high chemical resistance, and has been previously used in micro-opto-electro-mechanical systems (MOEMS). It is routinely used for lithographic patterning on the micro- and nanoscale, and hence beneficial for the creation of small structures. Silicon and Germanium carriers were used as readily available bulk substrates that are widely used in microfabrication of electronic and photonic devices, thus for which a large number of microfabrication processes are known.

When using polymers as donor material, photophysical effects as damage mechanisms need to be considered during transfer, and these mechanisms include photochemical decomposition, thermal ablation, spallation and photopolymerisation of monomer chains [35,36]. The use of short pulses and infrared wavelength decrease the likelihood of damage via thermal effects or direct rupture of polymeric bonds respectively, while multiphoton effects would only be expected for the highest fluences used. At the same time, thermal effects to the semiconductor carriers are expected to be reduced with short laser pulses when compared to longer pulsed laser sources, and this has further motivated our choice of laser source for these experiments [37].

With the help of a time-resolved shadowgraphy setup, we have recorded the position of the emerging flyer as a function of pulse energy, donor thickness, carrier material, delay time after laser pulse arrival, and beam intensity distribution. Shadowgraphy can be used to determine the existence and position of particles and flyer ejected from the donor surface and is also sensitive to changes in the refractive index of the surrounding atmosphere, e.g. through gradients in pressure or gaseous elements. Generally, shadowgraphy can be most readily performed with the presence of a receiver to study impact and landing of the flyer, and the receiver's interaction with pressure waves. Instead we have chosen to study the dynamics of the flyer ejection without receiver which is a case relevant to the LIBT process as the velocity, integrity and orientation of the flyer, and the possible creation of debris or shock can be observed over a larger range than possible with a receiver in place. In the following we refer to 'transfer' for the dynamics of flyer ejection and propagation for targets in a LIBT configuration as used here. To allow a more direct comparison with the LIBT process, we have briefly contrasted the results from shadowgraphy with those of standard transfer experiments, where we have measured the ratio of intact flyers found on a receiver to flyers imaged in an intact state.

We will first introduce the experimental details and methods of the time-resolved studies of LIBT. Then we present experimental results from varying time delay, laser fluence, donor thickness and carrier. Further, we will discuss the different observed transfer regimes and the effects of experimental parameters on LIBT of SU-8.

2. Experimental

The imaging of the LIBT process was carried out using the setup shown in Fig. 2. It consisted of three different optical beam lines, one for live imaging of the sample surface, one for laser-induced transfer and the third one for time-resolved shadowgraph imaging. Transfer was induced via pulses from a Ti:sapphire laser oscillator-amplifier system (Mira/Legend, Coherent) with a central wavelength of 800 nm, and pulse lengths of 150 fs. The maximum pulse energy of 2 mJ was attenuated with a continuously variable

neutral density filter. The Gaussian intensity profile from the laser was transformed into a top-hat intensity profile via a refractive beam shaper (Pi-Shaper, AdlOptica). These laser pulses with top-hat profile then illuminated the surface of a 608 × 684 element digital micromirror device (DLP3000, Texas Instruments) whose mirrors were actuated to form a dynamic intensity mask. To do so, mirrors in the 'on' position directed light into the beam path shown in Fig. 2, while mirrors in 'off' position steered the laser pulses into a beam stop (not shown). The surface of the digital micromirror device (DMD) displaying a user-specified mask was imaged and de-magnified at the interface between the donor and carrier in the LIBT target with a 50× de-magnification microscope objective (Mitutoyo).

For sample positioning and focussing, the sample, illuminated with a white light source, is imaged continuously on a CMOS camera, whose image path is collinear to the laser beam path. More details on the setup and on the configuration of the DMD for image projection can be found in previous work [38].

The laser-induced events above the sample surface were recorded via illumination from a white light spark discharge flash lamp (Nanolite KL-K, HSPS) with a pulse duration of 8 ns [39]. The flash lamp was placed at the focus of microscope objective L1 (10× magnification, Leitz Wetzlar) used as a collimator. A second microscope objective L2 (50× magnification, Nikon) was used to concentrate the illuminating light at the interaction area. The interaction of the illuminating beams and the laser-induced objects or differences in refractive indices were then observed as intensity gradients [40] on a CCD camera (scA1400–17 fm, 1.4 Mpx, Basler AG) equipped with a microscope objective L3. Depending on the resolution required and the field of view, we used one of two different (20× and 100× magnification, Nikon) microscope objectives L3. Our setup therefore provided the following theoretical resolutions: 90 nm/pixel and 420 nm/pixel, while the field of view in the direction of flyer movement equalled approximately 120 μm and 400 μm respectively. The excitation laser, flash lamp, shutter and the CCD camera were synchronised by a signal generator (Tektronix, AFG 3102) while the display of the DMD image mask, laser triggering and attenuation level were controlled by a computer.

Following laser triggering, the signal generator caused the CCD camera to be active for ~20 ms and at the same time actuated the flash lamp at a chosen delay time with a minimum value of 1.4 μs. A snapshot was therefore taken after the chosen delay with an exposure time of ~8 ns. We varied this delay during experiments over the range between 1.4 μs and 16.4 μs with an estimated uncertainty of 100 ns. For each delay a new area of the donor was selected, so the data presented below consists of sequential flyers imaged at different delays but otherwise similar conditions. To reduce errors due to natural fluctuations in flyer behaviour, each set of similar conditions was repeated at least five times. The delay was chosen to show flyers travelling the full extent of the image frame visible to the camera.

Fig. 3a shows a schematic of the imaging setup and the image shown in Fig. 3b is a typical shadowgram recorded with the CCD

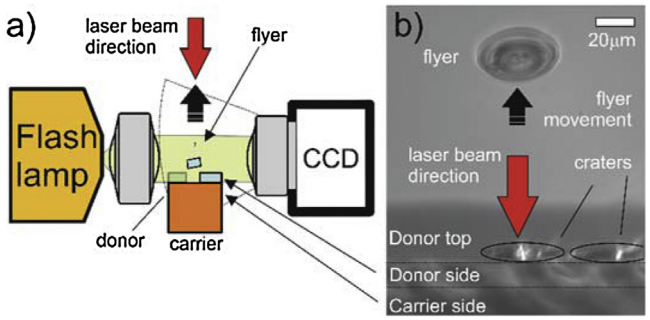

Fig. 3. (a) Schematic side-view of shadowgraphy imaging setup and (b) image frame as recorded by CCD camera and a 100× microscope objective.

camera where flyer and donor surface orientation appear at an angle relative to each other as a result of camera perspective. The contrast, brightness and gamma values of the captured images were modified to optimise visibility of the laser-induced events.

The LIBT targets (i.e. the donor-coated carrier) were fabricated via spin-coating of SU-8 photoresist (Microchem) onto silicon and germanium carrier substrates (300–600 μm thick). The germanium carriers consisted of a 3 μm thick layer of Ge grown on a Si substrate. Before spin-coating, the carriers were ultrasonically cleaned in sequential baths of acetone, isopropanol and water for 30 min and subsequently dried by pressurised nitrogen. After coating, the LIBT targets were baked on a hotplate for 3 min ramping from 60 to 90 °C, and the sample was held at 90 °C for a further minute to solidify the polymer and to remove any residual gamma-butyrolactone solvent [41]. Final donor thicknesses were 3.8 μm (referred to later as 'thin') and 6.4 μm (referred to as 'thick'), measured with a mechanical profiler. The variation of donor thickness measurement was in the range of ±100 nm while the measurement error by the mechanical profiler used was estimated to be smaller than this variation. The films were coated at spin speeds of 2000 rpm and 4000 rpm for maximum accelerations of 300 rpm/s and a spin duration of 30 s. The film thickness of a few microns was a typical thickness used in SU-8 based MEOMS and around the standard thickness for SU-8 5 used in lithography.

The targets were then cleaved in the centre for better imaging of the central part of the donor to avoid shading by the thick donor bead found at the perimeter of a spin-coated sample and experiments were performed at least 100 μm away from the sample (donor) edges to avoid variation of material properties, such as a reduced donor-carrier adhesion.

3. Results and discussion

3.1. Velocity of the flyer

In the first experiments we varied the delay between values of 1.4–10 μs between incidence of the laser pulse and recording of the position of the flyer above the substrate. A sequence of images

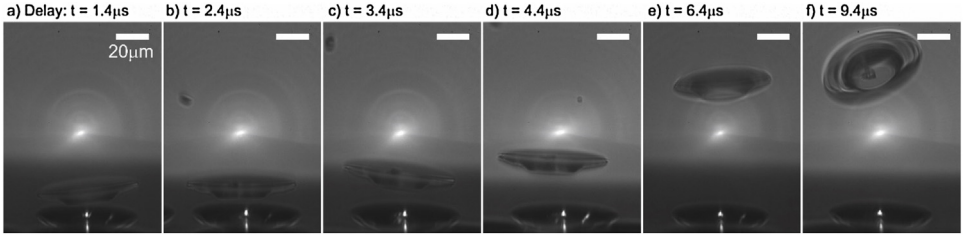

Fig. 4. Time sequence of shadowgrams of flyers from a thick SU-8 donor on a Si carrier imaged with a 100 x microscope objective. The scale bar is 20 μm in all figures.

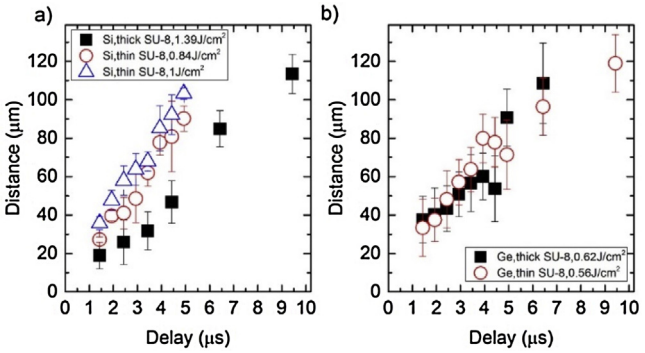

Fig. 5. Distance travelled by flyers for varying delay times from (a) Si and (b) Ge carriers with thick and thin SU-8 donors. The error bar is the standard deviation at a certain delay time.

taken for different delays at a fluence of 1.39 J/cm^2 for flyers from a thick SU-8 on silicon target are shown in Fig. 4.

A flyer emerges from the surface not as a cylindrical disc which could be the circular shape with top-hat spatial intensity projected at the interface, but is slightly tapered and additionally features a thin peripheral rim ripped out of the donor to result in a 'saucer-like' structure. Most of the shadowgraph images show two bright areas, one in the centre of the image and a second one in the crater on the donor. The first spot originates from direct imaging of the spark gap illumination, and while the presence of this bright spot in the image was undesired, this geometry was used to maximise flyer illumination. The second spot is a consequence of scattering of the laser pulse visible due to the long exposure time of the CCD camera.

The image also reveals that the bottom side of the tilted flyer carries some damage appearing in the central region of the flyer. This damage, seen as dark spots within a flyer, occurred to some of the flyers and was most likely caused by imperfections of the donor or fluctuations of the laser pulse intensity due to imperfect optics or laser output. As flyers were not collected, further evaluation of this damage was not possible. The particles shown in Fig. 4b–d is debris which likely has its origin in the central damaged spot of the flyer.

Experiments were carried out just above flyer removal fluence thresholds for the 3.8 μm and 6.4 μm thick films. For donors on silicon these threshold fluences were between 0.80 J/cm^2 and 1.35 J/cm^2 as a function of donor thickness. Germanium carriers had threshold fluences between 0.55 J/cm^2 and 0.60 J/cm^2. The differences in threshold fluences observed between experiments with the different carrier substrates could be reduced to both the different physical properties of the carrier or to the different adhesion of donor on carrier, and further measurements of adhesion would be required to determine the effect of these properties.

The distance d travelled by the resulting intact flyers for an image taken after a specific delay is shown in Fig. 5.

Experiments for thin SU-8 on silicon were performed at fluences just above and at 20% higher than threshold for comparison to see if there is a measurable influence of fluence on velocity. The higher value was chosen to be between the threshold and the fluence at which the likelihood of breaking up would increase dramatically. The velocity $v(t)$ of a flyer as a function of delay t as shown in Table 1 and Fig. 6 was defined as:

$$v(t) = \frac{d(t) - d(t_1)}{t - t_1} \quad (1)$$

with t_1 the minimum delay (1.4 μs). From previous experiments, it is expected that flyer ejection (occurring at time t_0) is initiated on the timescale of hundreds of nanoseconds after laser pulse arrival and is a function of fluence [42,43]. Generally, using short pulses

Table 1
Intact flyer velocities for different carrier/donor combinations extracted from distance vs. delay data. The fluence values for the samples are shown in Fig. 5. The temporal mean of the velocity is shown for different fluences and combinations of donor and carrier.

Carrier/Donor (Fluence)	Mean velocity [m/s]
Si/Thin SU-8 (0.84 J/cm^2)	18.1 ± 2.1
Si/Thin SU-8 (1 J/cm^2)	19.8 ± 2.3
Si/Thick SU-8	9.3 ± 2.8
Ge/Thin SU-8	13.5 ± 1.5
Ge/Thick SU-8	9.1 ± 5.4

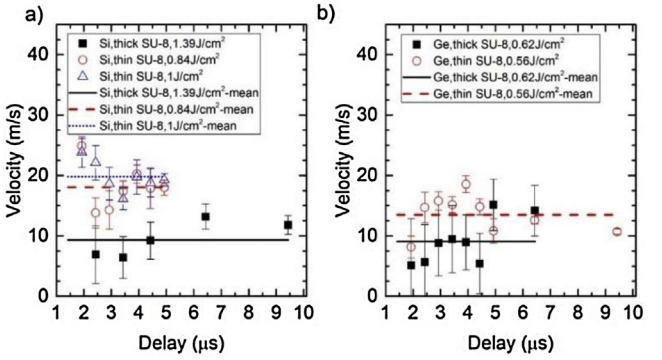

Fig. 6. Velocity as a function of delay time for (a) silicon and (b) germanium carriers with thin (3.8 μm) and thick (6.4 μm) SU-8 donors.

and higher fluences can decrease t_0. However, the influence of dynamic release layers (DRL) such as Au [44] is inconclusive, while for a Triazene DRL [45], a thicker film can decrease t_0 significantly as compared to a thin DRL [43]. While the pressure of the surrounding atmosphere does have a large effect on propagation velocity, no major influence on ejection time could be observed in literature [33].

Resulting mean velocities for flyers were in the range of 9–20 m/s, and the lowest velocity recorded was 6 m/s. For both carriers, the thicker flyers had a lower velocity than the thin flyers. The comparison of a thin flyer from a Si carrier in Table 1 shows slightly higher velocities for a flyer ejected at 20% higher fluence but otherwise similar conditions for the mean velocity. Fig. 5 also shows that flyers ejected at higher fluence have always travelled further at comparable delay times, hinting at a smaller flyer release time t_0 for higher fluences. The velocities as a function of delay are plotted in Fig. 6.

No indication of any deceleration, e.g. by drag, could be seen in the velocity over the time delays studied. The flyer propagation was assumed to be influenced by the deceleration through the surrounding atmosphere as well as by the flyer rotation induced during flyer ejection. Gravity acting in the opposite direction of travel was neglected being several orders of magnitude smaller than drag from the surrounding air at atmospheric pressure. The different flyer velocities observed are crucial to estimate the outcome of a LIBT experiment as a higher velocity increases the impact when landing on a receiver.

3.2. *Influence of laser fluence on flyer propagation*

As observed in Fig. 5 for the thin donor films, distance travelled in a specific time period increased for higher laser pulse energies incident on the targets as seen earlier [46]. This relation was investigated in more detail by recording flyer propagation for a fixed delay time but varying laser fluence for Ge and Si carriers. Fig. 7 shows the resulting behaviour for flyers from a thick SU-8 donor and a Ge carrier.

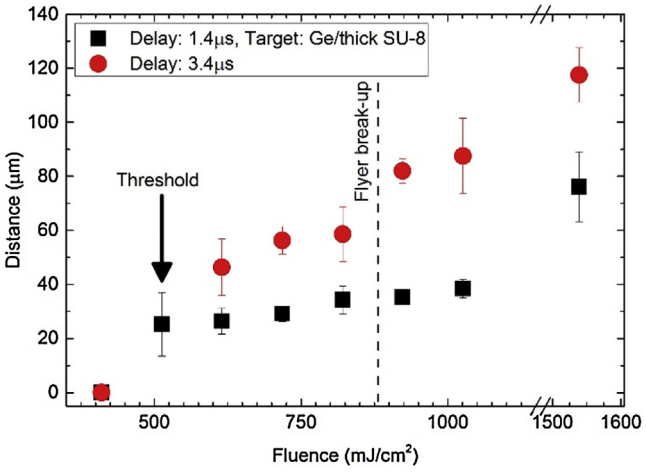

Fig. 7. Distance travelled by flyer for two delay times when varying incident pulse fluence for a Ge carrier and a thick SU-8 donor film. The first data points at ~400 mJ/cm^2 show that no flyer had emerged from the donor.

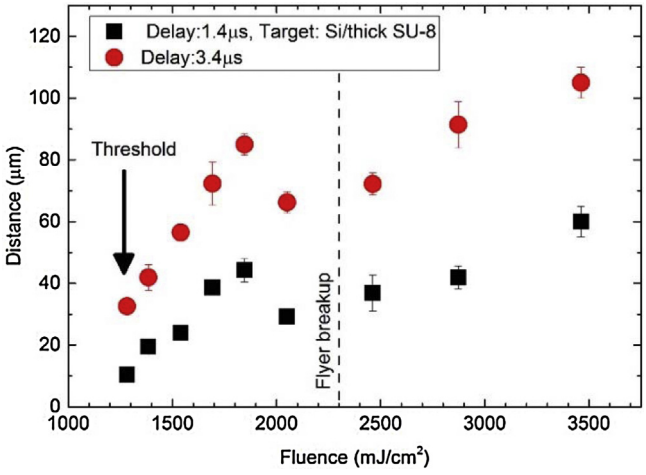

Fig. 8. Distance travelled as a function of incident laser fluence for a flyer from a thick SU-8 donor on Si carrier.

During this experiment only flyers up to a fluence of 0.9 J/cm^2 and 2.3 J/cm^2 for Ge and Si carriers respectively were observed to be in an intact state. For higher fluences, more than 90% of flyers were found to have fragmented. The distances plotted at larger fluences show the distance travelled by the main fragments ejected from the donor surface. Before breakup, the measured average velocities of the fastest flyers were 12.2 ± 7.7 m/s. The error found for these fastest flyers was relatively large and we assumed that the tilt of some of the recorded flyers may have contributed to their deceleration. For a germanium carrier, all flyers ejected at a high fluence travel further, thus at a higher average velocity, than flyers ejected at a lower fluence close to threshold. The resulting linear increase of velocity as a function of fluence was in the range of 0.023 ± 0.01 m/s mJ^{-1} cm^2 for flyers in an intact state.

A similar plot of distance over delay time from an experiment with silicon carriers is shown in Fig. 8. Here, the distance curves are split at a fluence value of ~1.8 J/cm^2 into a 'sawtooth' function with positive gradients. The first part of the fitted sawtooth function (1.25–1.8 J/cm^2), showing the distances of intact flyers, has a gradient of velocity of 0.014 ± 0.01 m/s mJ^{-1} cm^2. The velocity of the fastest flyers here was 16.8 ± 4.6 m/s.

In the first part of the curve, distance increases monotonically. However, around 2.0–2.5 J/cm^2, propagation is much lower than expected. Only for values of 3.5 J/cm^2 is propagation again larger

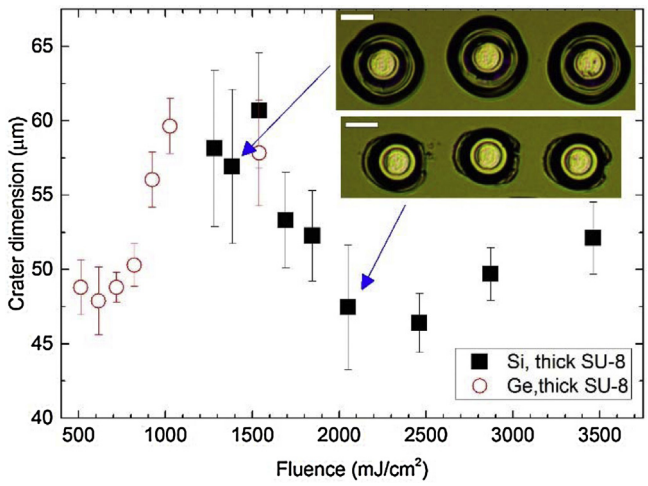

Fig. 9. Crater diameter for varying fluence measured on two Si and Ge donors after LIBT experiments for a thick SU-8 donor. The insets shows microscope images of craters in the donor after transfer (for Si carrier). The scale bar of the insets is 25 μm.

than for flyers ejected at 1.8 J/cm^2. Such behaviour would seem to indicate a deceleration or a change of transfer regime for those higher fluences. To further investigate this behaviour, we have measured the diameter of the ablation craters in the donor films left behind by the ejected flyer as shown in Fig. 9.

For a fixed image mask as used throughout this experiment, it was expected that crater size would remain constant or increase only slightly for increasing fluence due to areas in the perimeter of the imaged mask feature, where intensity, decaying in an exponential fashion due to imperfect imaging, exceeded the transfer threshold, resulting in a larger flyer being ejected. However, Fig. 9 shows a local minimum in crater size for SU-8/Si targets at around 2.5 J/cm^2 confirming that craters, and as a consequence flyers, do not have a constant or linear increasing diameter.

The beam diameter at the donor-carrier interface was ~20 μm, estimated from microscope images of the donor damage at low fluences. From Fig. 9 and previous experiments we can see that the flyer shape is much larger. During flyer release, the flyer shears off additional neighbouring donor areas and thus results in an increase in flyer diameter. Although an exact cause of the observed variation in flyer diameter is difficult to confirm, we assumed that different factors could contribute to the observed flyers shape distribution. It had been observed earlier in polymers that higher impact velocities on polymer can lead to different failure modes [47]. Slow donor loading would induce brittle fracture (tensile failure mode) while fast loads would induce a transition to a ductile (failure) regime where shear crack growth is preferred. Thus a fast 'push' could lead to a different transfer regime preferring straight edges in crater and resulting flyer. This different failure mechanism would then cause a different amount of kinetic energy to be delivered to the flyer during flyer ejection or on the other hand the donor accelerated at different rates would suffer from these different failure regimes. The effect of varying crater size and velocity was not seen in the experiments with Ge carrier and hence could be a consequence of the relatively high fluences required for the Si carriers. In general, the failure mode determines the resulting flyer edge quality and shape. Additionally, the increased fluence could increase the likelihood of non-linear multiphoton absorption, shock-induced changes [48] or even heating of the flyer and hence its change in global or local mechanical properties explaining the observed changes in flyer and crater shape.

From our experiments here, we can also estimate the influence of the receiver by determining the fluence window *FW*, in which flyers are either seen intact for shadowgraphy experiments,

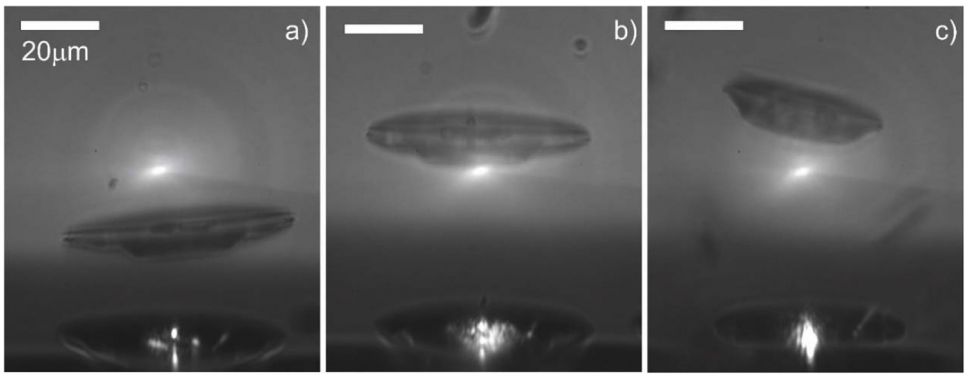

Fig. 10. Shadowgraph image of flyers ejected from a thick SU-8 film on a silicon carrier ejected at (a) 1.39 J/cm^2, (b) 1.69 J/cm^2, and (c) 2.05 J/cm^2 respectively. Delay times were 3.4 μs. Images were taken via a 100× objective. The scale bar is 20 μm in all figures.

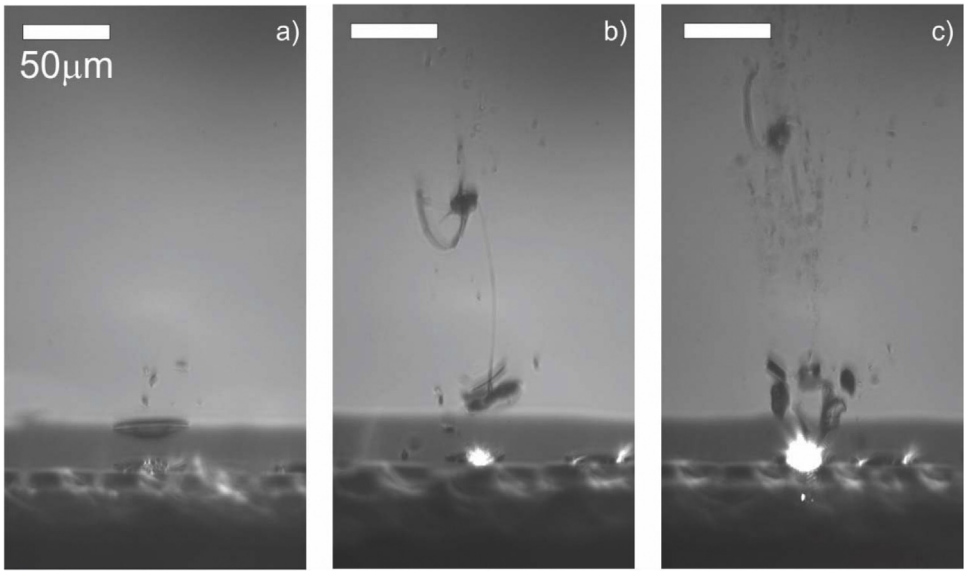

Fig. 11. Shadowgraph images from LIBT events of a thick SU-8 donor on silicon carrier. Fluences were (a) 1.39 J/cm2, (b) 2.05 J/cm2, and (c) 3.46 J/cm2. Images were taken with a CCD mounted 20 x objective and delay was 2.4 μs. The scale bar is 50 μm in all figures.

or intact for LIBT experiments printing onto a receiver. This results in a transfer window defined as:

$$FW = \frac{F_u - F_{th}}{F_{th}} \quad (2)$$

with F_u and F_{th} the respective maximum and minimum fluence for which flyers are ejected or deposited in intact state. *FW* for thick flyers on Ge and Si was approximately 60%. For comparison, in an experiment using a polydimethylsiloxane-coated glass receiver and a thin SU-8 donor from a Si carrier (flyers in transfer were not imaged), *FW* was ~16%, compared to ~38% for shadowgraphy experiments, for flyers ejected from the donor. This indicates that the influence of the receiver contributes to a reduction of this transfer window by approximately a factor of two (≈38%/16%). As shown previously for LIFT, the reduction of transfer window can be explained by shock waves reflecting off the surface of the receiver [33] or destruction due to impact on the receiver [49]. Further, it may as well be possible that the receiver might cause aberrations leading to imperfect imaging of the object at the image plane which in turn would increase the likelihood of fractured flyer ejection.

3.3. Transfer regimes of flyers

The influence of laser pulse energy, and thus fluence delivered to the LIBT target, on the velocity and shape of a flyer, is further shown in images of flyer ejection events. Fig. 10 shows shadowgraphs taken with a 100× objective from a thin SU-8 on silicon target at delays of 3.4 μs. For the selected fluences of 1.39 J/cm^2, 1.69 J/cm^2 and 2.05 J/cm^2 propagation distance is described approximately by the data presented in Fig. 8.

The flyers with the same conditions as for the one shown in Fig. 10c have a different profile compared to the other flyers confirming the data of crater diameter shown in Fig. 9. They have a smaller diameter and appear to miss the thin rim seen in the other flyers of Fig. 10. However, they only propagate to a distance similar to a flyer ejected at a fluence of 1.69 J/cm^2, hence not all the excess energy deposited into the target is used for acceleration of the flyer in a direction away from the donor.

When using an objective with 20× magnification with a thick SU-8/Si target, debris distribution and fast particles can be better detected due to the larger field of view. Fig. 11 shows transfer events for low (1.39 J/cm^2), medium (2.05 J/cm^2) and high (3.46 J/cm^2) fluences. Note that for these medium fluences, intact flyers only occurred in ~50% of transfer events and were never seen for high fluences.

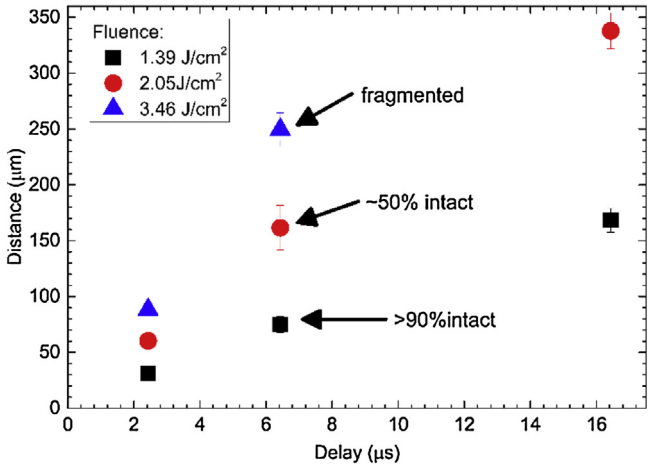

Fig. 12. Distance versus delay for thick SU-8/Si and different transfer regimes. Note that for the two higher fluences, distance values are shown for the main fragments, while for the lowest fluence, only intact flyers are shown.

For low fluences in more than 90% of the cases, the flyer was intact. As shown in Fig. 11, small amounts of debris presumably from the perimeter of the sheared flyer are visible. As the flyer appears to be slightly smaller than shown in Fig. 9, we assumed that one of the sources of such debris is the perimeter of the flyer. For medium fluences as for the flyer in Fig. 11b, disintegration of the main flyer is apparent at a distance of around 50 µm, the number of small particles or debris has increased, and at the centre of the image, an additional compact and relatively large feature can be seen which is connected with a long string of material to the lower, main flyer. Such a string or jet is an indicator of molten material and could explain the saturation of the main flyer velocity caused by a change in donor material phase and hence different mechanical properties [50]. Also, melting of the carrier at these relatively large fluences is likely to occur.

For high fluences, the molten features are still visible in the upper part of the image together with a large quantity of small particles. The main flyer is seen to have broken up in several pieces in a typical fashion for non-intact transfer. For the two higher fluences, seen near the crater, residual light emission is visible, originating from the incident laser pulse as the relatively long camera exposure time includes both laser pulse and flash lamp pulse events.

Fig. 12 emphasises further the different transfer regimes by showing propagation distances of intact flyers and large fragments of the main flyer. The largest extracted velocities for fragments seen at high fluences was ~40 m/s.

4. Conclusions

We have demonstrated the time-resolved shadowgraph imaging of thin transparent epoxy-based polymer SU-8 films via femtosecond laser-induced backward transfer. Flyer velocity, transfer regimes and intact transfer window were determined for different thicknesses (3.4 µm and 6.8 µm), delay times (1.4–16.4 µs) and carrier substrates of silicon and germanium for fluences of 0.5–3.5 J/cm^2. Observed velocities were in the range of 6–20 m/s for different donor thicknesses, carriers and laser fluences. We have seen that flyer velocity is a function of laser fluence with a gradient of 0.023 ± 0.01 m/s mJ^{-1} cm^2 for Ge and 0.014 ± 0.01 m/s mJ^{-1} cm^2 for Si carriers in intact state and flyers removed around threshold fluence. However, for Si carriers and large fluences, the crater found in the donor, the flyer shape and reduced flyer propagation velocity indicate a different flyer failure regime than for low fluences. Also, we have not detected any shock waves which are known to compromise flyer integrity during LIFT experiments. The receiver has shown to be responsible for a reduction of the fluence transfer window by approximately a factor of two. Among the tested carriers, due to their relatively low ejection threshold a germanium carrier is preferred over the silicon one. These findings are helpful for better understanding of the LIBT process, for e.g. future modelling, and to determine experimental parameters for LIBT printing intact deposits.

Acknowledgements

This work was funded under the UK Engineering and Physical Sciences Research Council (EPSRC) Grants Nos. EP/L022230/1 and EP/J008052/1. The authors also would like to acknowledge financial support from the state budget by the Slovenian Research Agency [Programme No. P2-0392]. Goran Mashanovich is kindly acknowledged for providing germanium samples. The data for this work are accessible through the University of Southampton Institutional Research Repository (DOI: 10.5258/SOTON/398008).

References

[1] M. Vaezi, H. Seitz, S. Yang, A review on 3D micro-additive manufacturing technologies, Int. J. Adv. Manuf. Technol. 67 (2013) 1721–1754, http://dx.doi.org/10.1007/s00170-012-4605-2.
[2] Y. Zhang, C. Liu, D. Whalley, Direct-write techniques for maskless production of microelectronics: A review of current state-of-the-art technologies, in: 2009 Int. Conf. Electron. Packag. Technol. High Density Packag., IEEE, 2009, pp. 497–503, http://dx.doi.org/10.1109/ICEPT.2009.5270702.
[3] A. del Campo, E. Arzt, Fabrication approaches for generating complex micro- and nanopatterns on polymeric surfaces, Chem. Rev. 108 (2008) 911–945, http://dx.doi.org/10.1021/cr050018y.
[4] J.A. Grant-Jacob, B. Mills, M. Feinaeugle, C.L. Sones, G. Oosterhuis, M.B. Hoppenbrouwers, R.W. Eason, Micron-scale copper wires printed using femtosecond laser-induced forward transfer with automated donor replenishment, Opt. Mater. Express 3 (2013) 747, http://dx.doi.org/10.1364/OME.3.000747.
[5] C.B. Arnold, P. Serra, A. Piqué, Laser direct-write techniques for printing of complex materials, MRS Bull. 32 (2007) 23–32, http://dx.doi.org/10.1557/mrs2007.11.
[6] A.J. Birnbaum, H. Kim, N.A. Charipar, A. Pique, Laser printing of multi-layered polymer/metal heterostructures for electronic and MEMS devices, Appl. Phys. A: Mater. Sci. Process. 99 (2010) 711–716, http://dx.doi.org/10.1007/s00339-010-5743-8.
[7] C.L. Sones, K.S. Kaur, P. Ganguly, D.P. Banks, Y.J. Ying, R.W. Eason, S. Mailis, Laser-induced-forward-transfer: a rapid prototyping tool for fabrication of photonic devices, Appl. Phys. A 101 (2010) 333–338, http://dx.doi.org/10.1007/s00339-010-5827-5.
[8] P. Serra, M. Colina, J.M. Fernandez-Pradas, L. Sevilla, J.L. Morenza, Preparation of functional DNA microarrays through laser-induced forward transfer, Appl. Phys. Lett. 85 (2004) 1639–1641, http://dx.doi.org/10.1063/1.1787614.
[9] M. Feinaeugle, C.L. Sones, E. Koukharenko, B. Gholipour, D.W. Hewak, R.W. Eason, Laser-induced forward transfer of intact chalcogenide thin films: resultant morphology and thermoelectric properties, Appl. Phys. A 112 (2013) 1073–1079, http://dx.doi.org/10.1007/s00339-012-7491-4.
[10] D. Munoz-Martin, C.F. Brasz, Y. Chen, M. Morales, C.B. Arnold, C. Molpeceres, Laser-induced forward transfer of high-viscosity silver pastes, Appl. Surf. Sci. 366 (2016) 389–396, http://dx.doi.org/10.1016/j.apsusc.2016.01.029.
[11] E. Breckenfeld, H. Kim, R.C.Y. Auyeung, N. Charipar, P. Serra, A. Pique, Laser-induced forward transfer of silver nanopaste for microwave interconnects, Appl. Surf. Sci. 331 (2015) 254–261, http://dx.doi.org/10.1016/j.apsusc.2015.01.079.
[12] M. Zenou, Z. Kotler, Printing of metallic 3D micro-objects by laser induced forward transfer, Opt. Express 24 (2016) 1431, http://dx.doi.org/10.1364/OE.24.001431.
[13] C.W. Visser, R. Pohl, C. Sun, G.-W. Römer, B. Huis in 't Veld, D. Lohse, Toward 3D printing of pure metals by laser-induced forward transfer, Adv. Mater. 27 (2015) 4087–4092, http://dx.doi.org/10.1002/adma.201501058.
[14] Bert Huis in 't Veld, L. Overmeyer, M. Schmidt, K. Wegener, A. Malshe, P. Bartolo, Micro additive manufacturing using ultra short laser pulses, CIRP Ann. – Manuf. Technol. 64 (2015) 701–724, http://dx.doi.org/10.1016/j.cirp.2015.05.007.
[15] D.J. Heath, M. Feinaeugle, J.A. Grant-Jacob, B. Mills, R.W. Eason, Dynamic spatial pulse shaping via a digital micromirror device for patterned laser-induced forward transfer of solid polymer films, Opt. Mater. Express 5 (2015) 1129, http://dx.doi.org/10.1364/OME.5.001129.
[16] J. Ihlemann, R. Weichenhain-Schriever, Patterned deposition of thin SiOX-films by laser induced forward transfer, Thin Solid Films 550 (2014) 521–524, http://dx.doi.org/10.1016/j.tsf.2013.10.128.

[17] A.I. Kuznetsov, A.B. Evlyukhin, C. Reinhardt, A. Seidel, R. Kiyan, W. Cheng, A. Ovsianikov, B.N. Chichkov, Laser-induced transfer of metallic nanodroplets for plasmonics and metamaterial applications, J. Opt. Soc. Am. B 26 (2009) B130, http://dx.doi.org/10.1364/josab.26.00b130.
[18] D.P. Banks, C. Grivas, J.D. Mills, R.W. Eason, I. Zergioti, Nanodroplets deposited in microarrays by femtosecond Ti:sapphire laser-induced forward transfer, Appl Phys. Lett. 89 (2006) 193107, http://dx.doi.org/10.1063/1.2386921.
[19] M.L. Levene, R.D. Scott, B.W. Siryj, Material transfer recording, Appl. Opt. 9 (1970) 2260, http://dx.doi.org/10.1364/AO.9.002260.
[20] U. Zywietz, A.B. Evlyukhin, C. Reinhardt, B.N. Chichkov, Laser printing of silicon nanoparticles with resonant optical electric and magnetic responses, Nat. Commun. 5 (2014) 3402, http://dx.doi.org/10.1038/ncomms4402.
[21] A.I. Kuznetsov, J. Koch, B.N. Chichkov, Laser-induced backward transfer of gold nanodroplets, Opt. Express 17 (2009) 18820, http://dx.doi.org/10.1364/OE.17.018820.
[22] A.I. Kuznetsov, C. Unger, J. Koch, B.N. Chichkov, Laser-induced jet formation and droplet ejection from thin metal films, Appl. Phys. A 106 (2012) 479–487, http://dx.doi.org/10.1007/s00339-011-6747-8.
[23] B. Liu, Z. Hu, Y. Che, Ultrafast pulsed laser micro-deposition printing on transparent media, in: Micromach, Micromachining and Microfabrication Process Technology XV (2010) 759002–759006, http://dx.doi.org/10.1117/12.842806.
[24] S.G. Koulikov, D.D. Dlott, Ultrafast microscopy of laser ablation of refractory materials: ultra low threshold stress-induced ablation, J. Photochem. Photobiol. A Chem. 145 (2001) 183–194, http://dx.doi.org/10.1016/S1010-6030(01)00581-0.
[25] P. Papakonstantinou, N.A. Vainos, C. Fotakis, Microfabrication by UV femtosecond laser ablation of Pt, Cr and indium oxide thin films, Appl. Surf. Sci. 151 (1999) 159–170, http://dx.doi.org/10.1016/S0169-4332(99)00299-8.
[26] H. Sakata, S. Chakraborty, M. Wakaki, Patterning of Bi2O3 films using laser-induced forward and backward transfer techniques, Microelectron. Eng. 96 (2012) 56–60, http://dx.doi.org/10.1016/j.mee.2012.02.002.
[27] A. Luches, S.A. Mulenko, V.P. Veiko, A.P. Caricato, V. Chuiko, Y.V. Kudryavtsev, A.V. Lopato, A.A. Petrov, F. Romano, D. Valerini, Laser-assisted synthesis of semiconductor chromium disilicide films, Appl. Surf. Sci. 253 (2007) 6512–6516, http://dx.doi.org/10.1016/j.apsusc.2007.01.023.
[28] V.P. Veiko, E. a. Shakhno, V.N. Smirnov, G.D. Nikishin, S.P. Rho, Laser ablation and local deposition: physical mechanisms and application for decontamination of radioactive surfaces, J. Korean Phys. Soc. 51 (2007) 345, http://dx.doi.org/10.3938/jkps.51.345.
[29] M. Feinaeugle, D.J. Heath, B. Mills, J.A. Grant-Jacob, G.Z. Mashanovich, R.W. Eason, Laser-induced backward transfer of nanoimprinted polymer elements, Appl. Phys. A. 122 (2016) 398, http://dx.doi.org/10.1007/s00339-016-9953-6.
[30] E.T. Karim, M. Shugaev, C. Wu, Z. Lin, R.F. Hainsey, L.V. Zhigilei, Atomistic simulation study of short pulse laser interactions with a metal target under conditions of spatial confinement by a transparent overlayer, J. Appl. Phys. 115 (2014) 183501, http://dx.doi.org/10.1063/1.4872245.
[31] D.A. Zayarnyi, A.A. Ionin, S.I. Kudryashov, S.V. Makarov, A.A. Rudenko, E.A. Drozdova, S.B. Odinokov, Specific features of single-pulse femtosecond laser micron and submicron ablation of a thin silver film coated with a micron-thick photoresist layer, Quantum. Electron. 45 (2015) 462–466, http://dx.doi.org/10.1070/QE2015v045n05ABEH015788.
[32] C. Zhang, J. Yao, S. Lan, V.A. Trofimov, T.M. Lysak, Effects of plasma confinement on the femtosecond laser ablation of silicon, Opt. Commun. 308 (2013) 54–63, http://dx.doi.org/10.1016/j.optcom.2013.06.052.
[33] R. Fardel, M. Nagel, F. Nuesch, T. Lippert, A. Wokaun, Laser-induced forward transfer of organic LED building blocks studied by time-resolved shadowgraphy, J. Phys. Chem. C. 114 (2010) 5617–5636, http://dx.doi.org/10.1021/jp907387q.
[34] J.P. McDonald, J.A. Nees, S.M. Yalisove, Pump-probe imaging of femtosecond pulsed laser ablation of silicon with thermally grown oxide films, J. Appl. Phys. 102 (2007), http://dx.doi.org/10.1063/1.2778740.
[35] P.E. Dyer, Excimer laser polymer ablation: twenty years on, Appl. Phys. A: Mater. Sci. Process. 77 (2003) 167–173, http://dx.doi.org/10.1007/s00339-003-2137-1.
[36] M. Malinauskas, M. Farsari, A. Piskarskas, S. Juodkazis, Ultrafast laser nanostructuring of photopolymers: a decade of advances, Phys. Rep. 533 (2013) 1–31, http://dx.doi.org/10.1016/j.physrep.2013.07.005.
[37] B.N. Chichkov, C. Momma, S. Nolte, F. vonAlvensleben, A. Tunnermann, Femtosecond, picosecond and nanosecond laser ablation of solids, Appl. Phys. A: Materi. Sci. Process. 63 (1996) 109–115.
[38] B. Mills, M. Feinaeugle, C.L. Sones, N. Rizvi, R.W. Eason, Sub-micron-scale femtosecond laser ablation using a digital micromirror device, J. Micromech. Microeng. 23 (2013) 35005, http://dx.doi.org/10.1088/0960-1317/23/3/035005.
[39] M.S. Rabasović, D. Šević, N. Lukać, M. Jezeršek, J. Možina, P. Gregorčić, Evaluation of laser-induced thin-layer removal by using shadowgraphy and laser-induced breakdown spectroscopy, Appl. Phys. A 122 (2016) 186, http://dx.doi.org/10.1007/s00339-016-9697-3.
[40] G.S. Settles, Schlieren and Shadowgraph Techniques: Visualizing Phenomena in Transparent Media, Springer-Verlag, Berlin, 2006.
[41] Microchem, SU-8 Data Sheets, 2016 http://www.microchem.com/Prod-SU8.htm.
[42] M. Feinaeugle, A.P. Alloncle, P. Delaporte, C.L. Sones, R.W. Eason, Time-resolved shadowgraph imaging of femtosecond laser-induced forward transfer of solid materials, Appl. Surf. Sci. 258 (2012) 8475–8483, http://dx.doi.org/10.1016/j.apsusc.2012.04.101.
[43] K.S. Kaur, R. Fardel, T.C. May-Smith, M. Nagel, D.P. Banks, C. Grivas, T. Lippert, R.W. Eason, Shadowgraphic studies of triazene assisted laser-induced forward transfer of ceramic thin films, J. Appl. Phys. 105 (2009) 113118–113119 http://link.aip.org/link/?JAP/105/113119/1.
[44] L. Rapp, C. Cibert, A.P. Alloncle, P. Delaporte, S. Nenon, C. Videlot-Ackermann, F. Fages, Comparative time resolved shadowgraphic imaging studies of nanosecond and picosecond laser transfer of organic materials, Xvii Int Symp. Gas Flow, Chem. Lasers, High-Power Lasers 7131 (2009) 71311L, http://dx.doi.org/10.1117/12.817481.
[45] R. Fardel, M. Nagel, F. Nuesch, T. Lippert, A. Wokaun, Shadowgraphy investigation of laser-induced forward transfer: front side and back side ablation of the triazene polymer sacrificial layer, Appl. Surf. Sci. 255 (2009) 5430–5434 http://www.sciencedirect.com/science/article/pii/S0169433208018035.
[46] T. Mattle, J. Shaw-Stewart, A. Hintennach, C.W. Schneider, T. Lippert, A. Wokaun, Shadowgraphic investigations into the laser-induced forward transfer of different SnO2 precursor films, in: Appl. Surf. Sci. Elsevier B.V., 2013 pp. 77–81 10.1016/j.apsusc.2012.11.146.
[47] K. Ravi-Chandar, J. Lu, B. Yang, Z. Zhu, Failure mode transitions in polymers under high strain rate loading, Int. J. Fract. 101 (2000) 33–72, http://dx.doi.org/10.1023/A:1007581101315.
[48] K. Brown, R. Conner, Y. Fu, H. Fujiwara, D. Dlott, Microscopic states of shocked polymers, AIP Conf Proc. (2012) 1593–1596, http://dx.doi.org/10.1063/1.3686589.
[49] M. Feinaeugle, P. Horak, C.L. Sones, T. Lippert, R.W. Eason, Polymer-coated compliant receivers for intact laser-induced forward transfer of thin films: experimental results and modelling, Appl. Phys. A 116 (2014) 1939–1950, http://dx.doi.org/10.1007/s00339-014-8360-0.
[50] T. Kumada, H. Akagi, R. Itakura, T. Otobe, M. Nishikino, A. Yokoyama, Non-thermal effects on femtosecond laser ablation of polymers extracted from the oscillation of time-resolved reflectivity, Appl Phys. Lett. 106 (2015) 221605, http://dx.doi.org/10.1063/1.4921854.